RSC Advances

PAPER

View Article Online
View Journal | View Issue

Cite this: *RSC Adv.*, 2023, **13**, 28703

First-principles insights into the C_6N_7 monolayer as a highly efficient sensor and scavenger for the detection of selective volatile organic compounds

Ruishan Zhang,†[a] Zihao Wang,†[a] Qihua Hou,[a] Xiaobo Yuan,[a] Yongliang Yong, *[ab] Hongling Cui[a] and Xinli Li[bc]

The design of new gas sensors and scavengers of volatile organic compounds (VOCs) is desirable for VOC enriching, separation and utilization. Herein, first-principles methods were performed to investigate the potential of C_6N_7 monolayers as highly efficient sensors and scavengers for selective VOCs (toluene, benzene, vinyl chloride, ethane, methanal, acetone, ethanol, and acetaldehyde). The physisorption of toluene, benzene, acetone, ethanol, acetaldehyde, and methanal has relatively high adsorption strength and can significantly tune the electronic properties and work function (Φ) of the C_6N_7, indicating that the C_6N_7 monolayer is highly sensitive and selective to these VOC gases. In addition, the desorption time of benzene, acetone, ethanol, acetaldehyde, and methanal is about 3, 0.4, 2.0×10^{-2}, 3.0×10^{-2}, and 3.6×10^{-5} s at 300 K, respectively, indicating that the C_6N_7-based sensor has high reusability at room temperature. The recovery time of toluene was about 7.8×10^{2} s at 300 K, showing disposable toluene gas sensing of the monolayer. Our work confirms that the C_6N_7 monolayer as a resistance-type and Φ-type gas sensor and scavenger is highly sensitive, selective and reusable for VOCs (benzene, acetone, ethanol, acetaldehyde, and methanol), but is a disposable toluene gas sensor and scavenger at room temperature.

Received 16th August 2023
Accepted 24th September 2023

DOI: 10.1039/d3ra05573f

rsc.li/rsc-advances

1. Introduction

The increased emissions of volatile organic compounds (VOCs) that result from human activities and geological hazards have an adverse influence on the environment and human health. A sensor for detecting VOCs has thus been found to be pivotal in various industries such as biomedical, environmental monitoring, food quality and safety, and promoting occupation health,[1–4] as high-performance VOC sensors can significantly improve the information collection and the accuracy of real-time accident forecasts. There are numerous gas-sensing methods such as electrochemical analysis, catalytic, quartz crystal microbalances (QCM), photo-ionization (PID), optical fiber, micro gas chromatography, and microelectromechanical systems applied for VOCs detection.[5–7] However, there are still some issues with the commercially available gas sensors (for example, the amperometric and conductometric types), such as poor selectivity and sensitivity, and unstable room temperature detection.[5,8] As the most common sensing techniques of electrochemical analysis, the chemiresistive gas sensors, which change their electrical resistance in response to changes in the nearby chemical environment, have the simplest design and shape factor, and their most important part is the gas-sensing material, which is well known to remarkably influence the gas-sensing performance.[8] The design of novel nanomaterials is therefore gaining extensive interest for developing high-performance VOC gas sensors.[5,8–12]

With the rapid development of two-dimensional (2D) nanomaterials, more and more 2D gas-sensing nanomaterials with high-performance have been discovered.[8–15] Particularly, due to its unique structure and properties, graphene has extensively been used in gas sensing materials.[16–22] However, the absence of band gap in graphene seriously impedes the applications of the pure graphene in gas sensing, which prompts us to modify the graphene properties and develop its derivatives that can be explored to resolve the limitations in graphene sensors.[19–22] More importantly, the gas sensors constructed from new C-based 2D monolayers that contain C-neighboring elements (such as B, N, Si and C) and have structural analogues of graphene have attracted more and more attentions due to their unique structural features, large surface-to-volume ratios, outstanding thickness-dependent physicochemical properties such as semiconducting properties with an appropriate bandgap, tunable surface functionalities, and solution phase

[a]School of Physics and Engineering, Henan University of Science and Technology, Luoyang 471023, China. E-mail: ylyong@haust.edu.cn
[b]Advanced Materials Science Innovation Center, Longmen Laboratory, Luoyang 471003, China
[c]School of Materials Science and Engineering, Henan University of Science and Technology, Luoyang 471023, China
† These authors contributed equally to this work.

production for scalable device fabrication.[13–16,23–25] In particular, CN based monolayers, which consists of only two earth-abundant elements (C and N) that implies they can be prepared at a low cost, have been theoretically predicted and experimentally synthesized *via* various methods to possess various structures with different C/N ratios.[26–33] Compared with the pure C-based nanomaterials, due to the electron-accepting ability and different atomic radius of N atoms, the incorporation of N atoms in C-matrix influences the electronic structures and tune the charge distribution *via* the formed C–N bonds, and thereby making the adjacent C atoms more reactive in gas adsorption.[25] In addition, the increasing of the N-to-C ration in carbon nitrides generates novel electronic features and chemical/physical properties such as the tunable nanopore size and band gap and adjustable conductivity, which are promising for key applications. In this context, the CN-based monolayers have been extensively used in gas sensing and exhibited high sensitivity and selectivity towards toxic gas and VOCs such as C_2N,[34–37] C_3N,[38–41] CN,[42–44] C_3N_2,[45] C_7N_6,[46,47] C_6N_7,[48] g-C_3N_4,[49,50] and BC_6N[51,52] monolayers, which further motivates people's enthusiasm to exploit new C_xN_y structures with high-performance gas sensing. In particular for the sensing of VOCs, Agrawal *et al.*[39] has confirmed that the C_3N monolayer has relatively high sensing performance for acetone and isopropanol detection, while Ma *et al.*[40] has predicted that the Cu-doped C_3N monolayer has promising potential for optical VOCs sensors. The g-C_3N_4 monolayer and its composites with metal and metal oxide were demonstrated to have comparatively better gas sensing performance for detecting and decontaminating VOCs (ref. 50 and reference literature therein). Further, the C_3N monolayers doped with B atoms (simply BC_6N) were compelling and feasible candidate for chemiresistive sensors for room temperature breath analysis of VOCs.[52]

After the prediction of a novel CN-based monolayer (C_6N_7)[53] that contains C–C bridged heptazine units, it was recently successful-synthesized by Zhao *et al.*[54] through thermal polymerization using oxalamide and urea. Then Bafekry *et al.*[55–57] and Mortazavi *et al.*[58,59] systematically studied the structural stabilities and electronic properties of the C_6N_7 structure, and modified its structural, electronic, magnetic, and mechanical properties *via* introduction of defects and impurities to make this material suitable for nanoelectronic and spintronic devices. As an interesting matter of fact, the successfully preparation of C_6N_7 with low-density nanoporous structure that effectively the active area and surface-related properties, graphite-like layered structure, high thermal/acid/chemical stability, and nonmetallic covalent semiconducting properties with tunable bandgap make the C_6N_7 monolayer be promising potential for toxic gas detection.[48] In addition, the excellent structural characteristics of C_6N_7 monolayers are analogous to the other C_xN_y monolayers[26–33] such as C_2N, g-C_3N_4, C_3N_2, and C_7N_6 monolayers, which have been demonstrated to be promising candidates for gas sensors to monitor toxic gases and VOCs.[34–48] However, to our best knowledge, the adsorption behaviors and gas-sensing properties of VOCs on the C_6N_7 monolayer for sensor exploration are still unknown, which motivates us to investigate the sensing performance and mechanism of the C_6N_7-based VOCs sensors.

In this work, using first-principles methods based on DFT, we comprehensively studied the adsorption behaviors and gas-sensing characteristics of some common VOCs, including toluene (C_7H_8), benzene (C_6H_6), vinyl chloride (C_2H_3Cl), ethane (C_2H_6), acetone (CH_3COCH_3), ethanol (C_2H_5OH), acetaldehyde (CH_3CHO), and methanal (CH_2O), on the C_6N_7 monolayer to exploit its potential for detecting and removing VOCs. We found that the VOC gas molecules are all physisorbed on the pure C_6N_7 monolayer, and most of the adsorption of VOCs can effectively modify the electronic and optical properties of the C_6N_7. Our research thus indicates that the C_6N_7 monolayer is suitable as high-efficient gas sensors and scavengers for VOCs such as benzene, acetone, ethanol, acetaldehyde, and methanal at room temperature. This work can provide an alternative for design of new gas sensors and scavengers for VOCs applications.

2. Computational methods

The geometrical optimizations and electronic properties calculations were carried out in the DMol^3 code within spin-polarized DFT methods.[60,61] The GGA within PBEsol functional was used to describe the exchange–correlation interaction,[62] and the Grimme method was used for describing the correction of van der Waals (vdW) interactions.[63] The interactions between electrons and ions were stated using DNP basis sets and DFT semi-core pseudopotentials (DSPP).[64] Brillouin zone was displayed using the Monkhorst pack grid of $15 \times 15 \times 1$ k-points.[65] Charge transfer and analysis were obtained from the Hirshfeld method.[66] When the energy converges of (1×10^{-5} Ha), the maximum force converges of (0.002 Ha Å^{-1}), and the maximum displacement of (0.005 Å) were satisfied, the structural optimization ended. A 20 Å vacuum was added to ignore the interactions between layers. The electron localization function (ELF) was calculated by CASTEP package with a kinetic-energy cutoff of 500 eV.[67]

3. Results and discussions

The C_6N_7 monolayer as substrate was optimized using a 2×2 supercell as shown Fig. 1a, and it has a lattice constant of $a = b = 11.72$ Å. As expected, the C_6N_7 monolayer is a semiconductor with a bandgap of 1.186 eV, which was shown in Fig. 1b. To obtain the most stable configuration of each VOC molecule adsorbed on the C_6N_7 monolayer, as many as possible adsorption sites such as top (Tx, x = 1–4), hollow (Hx, x = 1,2) and bridge sites (Bx, x = 1–3) that were shown in Fig. 1a along with all possible different orientations of molecule referring to the monolayer surface were explored in this work. The most stable and second low-lying structures and of VOC molecules on the C_6N_7 monolayer were exhibited in Fig. 2 and 3, respectively, while their corresponding calculated results were listed in Table 1. To illustrate clearly, the most stable state for each VOC on the monolayer was called as molecule-1 for short, while the molecule-2 denotes the second most stable adsorption state.

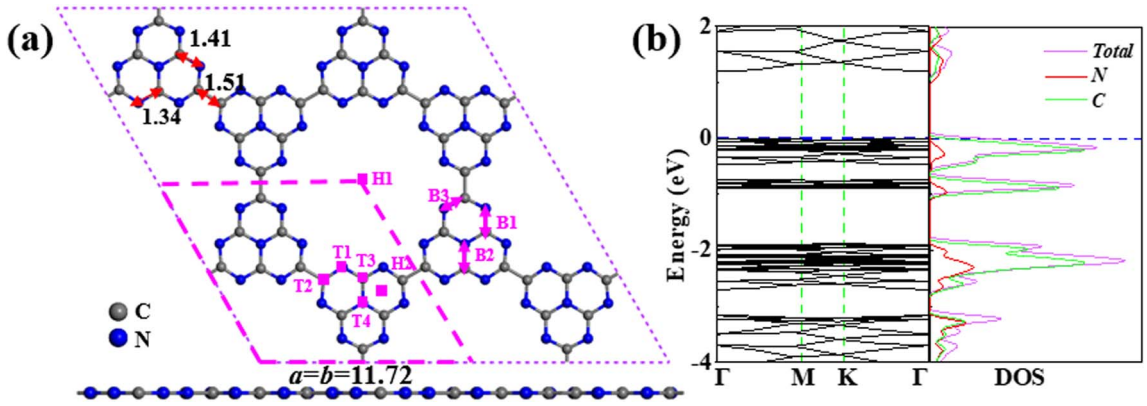

Fig. 1 (a) The configuration of the C_6N_7 monolayer, and (b) the corresponding band structure and DOS. The adsorption sites are labeled in (a) as T*x*, B*x*, and H*x* ($x = 1$–4). The lengths in (a) are in Å.

For the adsorption of toluene on the C_6N_7 monolayer, the most stable adsorption position of toluene is located at the top of the heptazine unit, which was shown in Fig. 2a (toluene-1), and it possesses an adsorption strength of −0.956 eV, which is more stable than that of other toxic gases on the monolayer.[48] The adsorption energy (E_{ad}) was calculated as $E_{ad} = (E_{total} - E_{mono} - nE_{mol})/n$, where E_{total}, E_{mono} and E_{mol} is the energy of the VOC-C_6N_7 compound, the C_6N_7 substrate, and the studied VOC molecule, respectively, and n is the number of VOC molecules. In addition, we also obtained the second stable configuration of toluene on the C_6N_7 as displayed in Fig. 3a (toluene-2) that owns an E_{ad} of −0.771 eV, higher in energy of 0.185 eV than the toluene-1 structure. Very different from the configuration of Toluene-1, the toluene in toluene-2 structure is located on the pore of the monolayer. As shown in Fig. 2b, the most stable adsorption site for benzene (benzene-1) with an E_{ad} of −0.787 eV is very similar to the case of toluene, however, in the second stable structure (benzene-2), the benzene is located

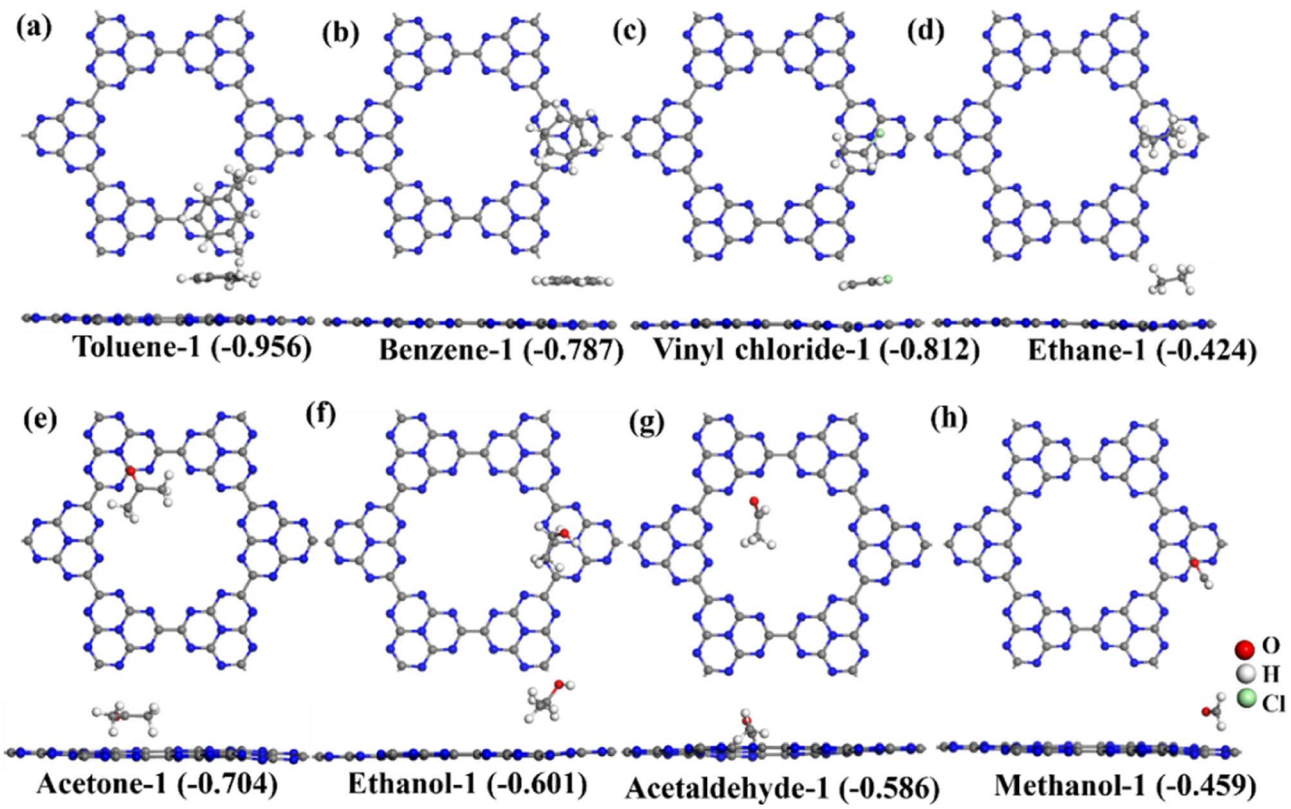

Fig. 2 The most stable configurations of VOC molecules adsorbed on the C_6N_7 monolayer: (a) toluene-1, (b) benzene-1, (c) vinyl chloride-1, (d) ethane-1, (e) acetone-1, (f) ethanol-1, (g) acetaldehyde-1, and (h) methanal-l. The corresponding adsorption energy was shown in parentheses (in eV).

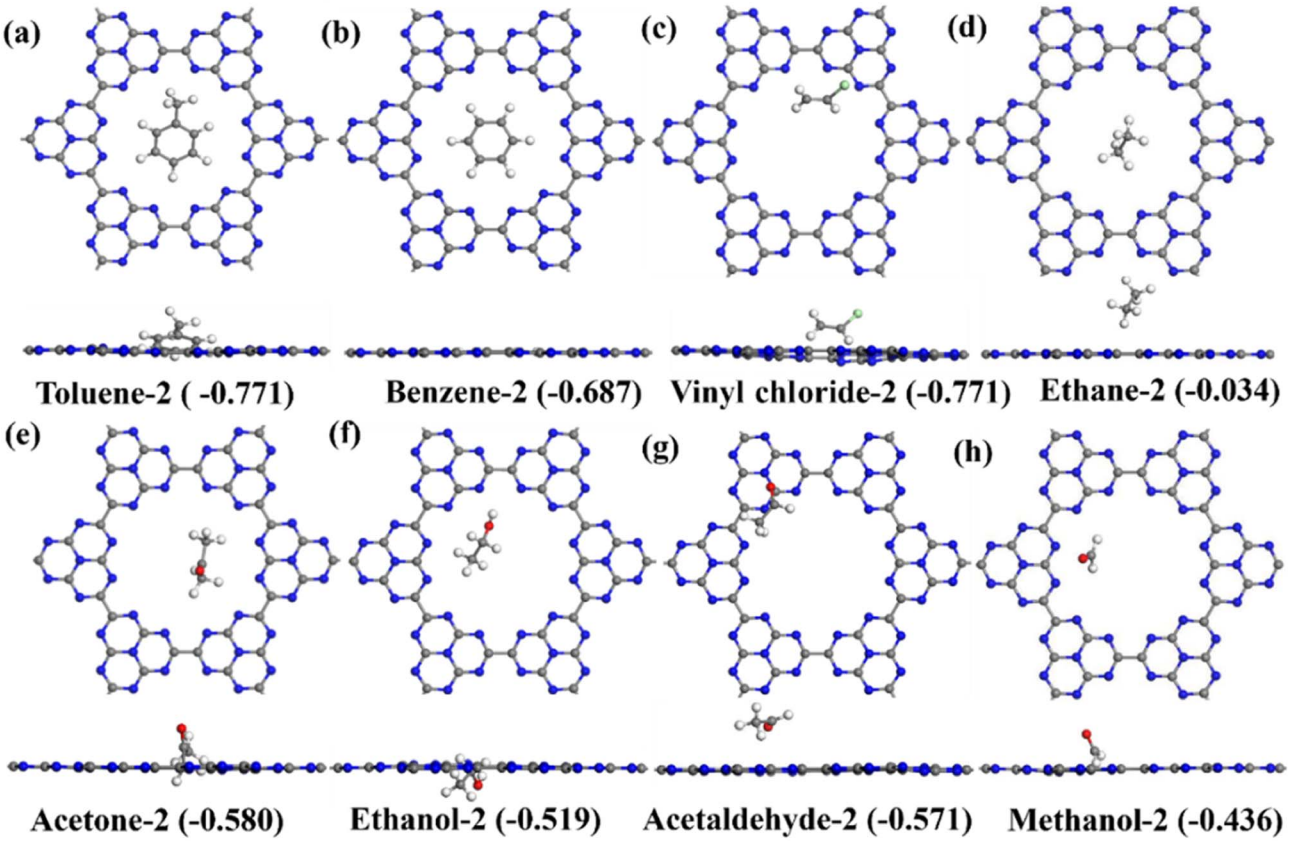

Fig. 3 The second most stable configurations of VOC molecule adsorbed on the C_6N_7 monolayer: (a) toluene-2, (b) benzene-2, (c) vinyl chloride-2, (d) ethane-2, (e) acetone-2, (f) ethanol-2, (g) acetaldehyde-1, and (h) methanal-2. The corresponding adsorption energy was shown in parentheses (in eV).

Table 1 Adsorption energy (E_{ad}), transferred charge (ΔQ) and the shortest distance (D) from molecule to monolayer, band gap (E_g), work function (Φ), and recovery time (τ) for VOC molecules adsorbed on the C_6N_7 monolayer

System	E_{ad} (eV)	ΔQ (e)	D (Å)	E_g (eV)	Φ (eV)	τ (s)
Toluene-1	−0.956	0.009	2.769	1.000	6.422	1.2×10^{4}
Toluene-2	−0.771	−0.09	—	0.003	5.415	9.1
Benzene-1	−0.787	0.014	3.025	1.157	6.585	16.4
Benzene-2	−0.687	−0.162	—	0	5.442	0.3
Vinyl chloride-1	−0.812	0.168	2.981	1.187	6.639	44
Vinyl chloride-2	−0.771	0.155	1.422	0.564	6.041	8.9
Ethane-1	−0.424	−0.048	2.564	1.191	6.612	1.3×10^{-5}
Ethane-2	−0.034	−0.004	2.998	1.185	6.639	3.8×10^{-12}
Acetone-1	−0.704	−0.071	2.734	0.313	5.605	0.7
Acetone-2	−0.580	−0.028	—	0.005	5.442	5×10^{-3}
Ethanol-1	−0.601	−0.060	3.226	0.778	6.258	2×10^{-2}
Ethanol-2	−0.519	−0.099	—	0.123	5.551	$5 \times 10–^{4}$
Acetaldehyde-1	−0.586	−0.014	—	0.136	5.578	6×10^{-3}
Acetaldehyde-2	−0.571	−0.015	3.184	0.811	6.232	3×10^{-3}
Methanal-1	−0.459	0.005	2.572	0.984	6.394	5.3×10^{-5}
Methanal-2	−0.436	−0.045	—	0.069	5.524	2.1×10^{-5}

in the pore, which was displayed in Fig. 3b, and this case is just less stable in energy of 0.1 eV than the most stable one. More importantly, there is a total of charge of 0.165 e transferred from the N atoms located at the pore edge to the benzene, which may be because of the electronegative N atom in pore edge. Further, we found that for the adsorption of vinyl chloride, ethane, and ethanol, the most stable configuration was formed by each molecule lying on the heptazine unit as displayed in Fig. 2c, d, and f, respectively.

For acetone adsorption, the most stable structure (acetone-1) has an E_{ad} of −0.704 eV as displayed in Fig. 2e, and in which the acetone is on the pore edge with the O in acetone pointing to a C atom in the pore edge of monolayer. However, when the acetone adsorbs on the top of the center of the pore as shown in Fig. 3e (acetone-2), its adsorption energy decreases to −0.580 eV, higher 0.124 eV than that of the most stable one. The adsorption of methanal as shown in Fig. 2h and 3h is very similar to the case of acetone. For the adsorption of acetaldehyde as shown in Fig. 2g, the most stable configurations (acetaldehyde-1) were formed by the molecule located at the top of the pore. On the contrary, in the second most stable structure for acetaldehyde adsorption as shown in Fig. 3g (acetaldehyde-2), the acetaldehyde molecule is basically located at the heptazine unit with E_{ad} of −0.519 eV, which is higher in energy of 0.015 eV than that of acetaldehyde-1 (−0.586 eV). The adsorption of ethane at the top of pore center just has an E_{ad} of −0.034 eV, which is too small to make the adsorption exist stably (see Fig. 3d).

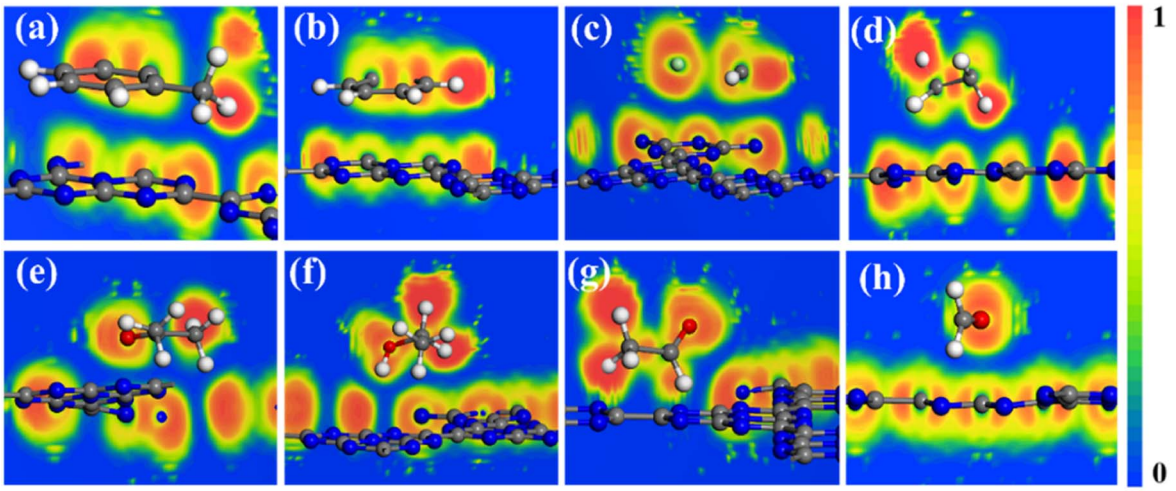

Fig. 4 The ELF plots for the most stable adsorption states of VOC molecules on the C_6N_7 monolayer: (a) toluene-1, (b) benzene-1, (c) vinychloride-1, (d) ethane-1, (e) acetone-1, (f) ethanol-1, (g) acetaldehyde-1 and (h) methanal-1.

We noted that the adsorption of these VOCs on the C_6N_7 surface has strong adsorption strength as the absolute E_{ad} value is larger than 0.6 eV as displayed in Fig. 2 expect for ethane and methanal. The adsorption of ethane and methanal has quite small absolute E_{ad} values, insignificant charge transfer, and large distance between molecule and monolayer, indicating the weak physisorption of ethane and methanal on the monolayer. To verify the adsorption type of toluene, benzene, vinyl chloride, acetone, ethanol, and acetaldehyde on the C_6N_7 monolayer, we calculated the ELF of these adsorptions, which were shown in Fig. 4. The ELF function, which can explain a great variety of bonding situations ranging from the most standard covalent bond to the metallic bond, has values in the range of 0–1, where 0 donates the nonbonding electron pairs or noncovalent interactions between atoms, while 1 denotes delocalization or covalent bonding. As clearly shown in Fig. 4, the ELF values between VOC molecules and the C_6N_7 monolayer are almost 0, powerfully supporting that the VOC molecules are all strongly physisorbed on the C_6N_7. However, the adsorption of the C_6N_7 monolayer towards the considered VOC molecules is much higher than that of other C-based monolayers such as C_3N,[39] BC_6N,[52] and C_2N as well as its heterostructure,[68] showing that the C_6N_7 monolayer has better potential in the adsorbents for removal these VOC gases.

In order to gain a deeper understanding of VOC molecules adsorbed on the C_6N_7 monolayer, their electronic properties were studied. Specifically, the band structures (BS) and density of states (DOS) along with the local DOS (LDOS) of molecules were shown in Fig. 5 and 6. We found that the adsorption of VOC molecules that were located at the top of heptazine unit

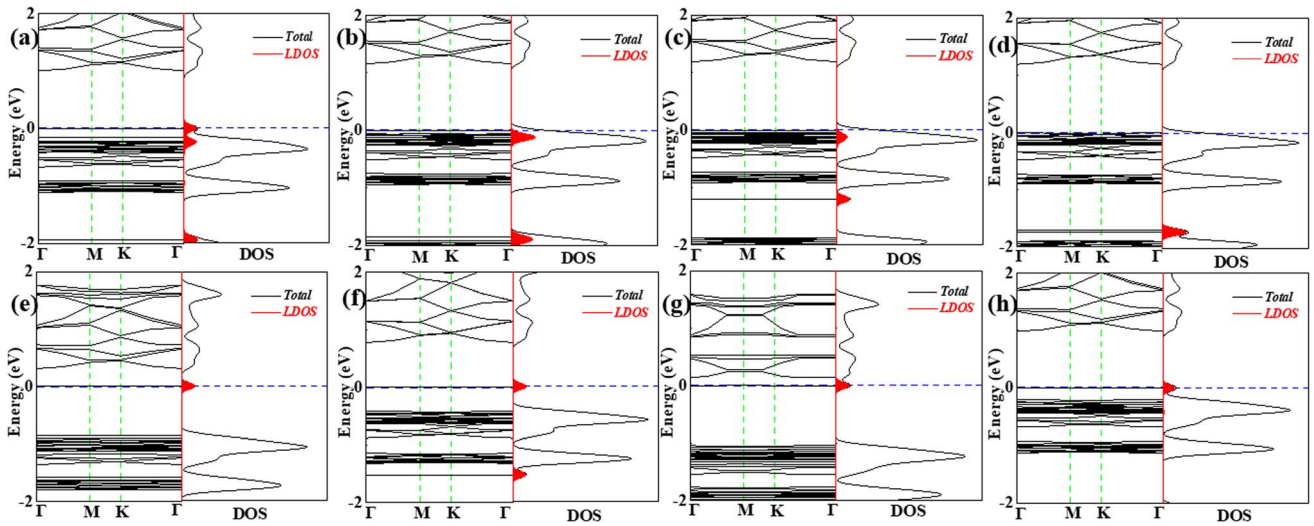

Fig. 5 The BSs and DOSs of the most stable structure of each VOC molecule on the C_6N_7: (a) toluene-1, (b) benzene-1, (c) vinyl chloride-1, (d) ethane-1, (e) acetone-1, (f) ethanol-1, (g) acetaldehyde-1, and (h) methanal-l. The local DOS (LDOS) of isolated molecules were marked as red under total DOS curves (dark lines).

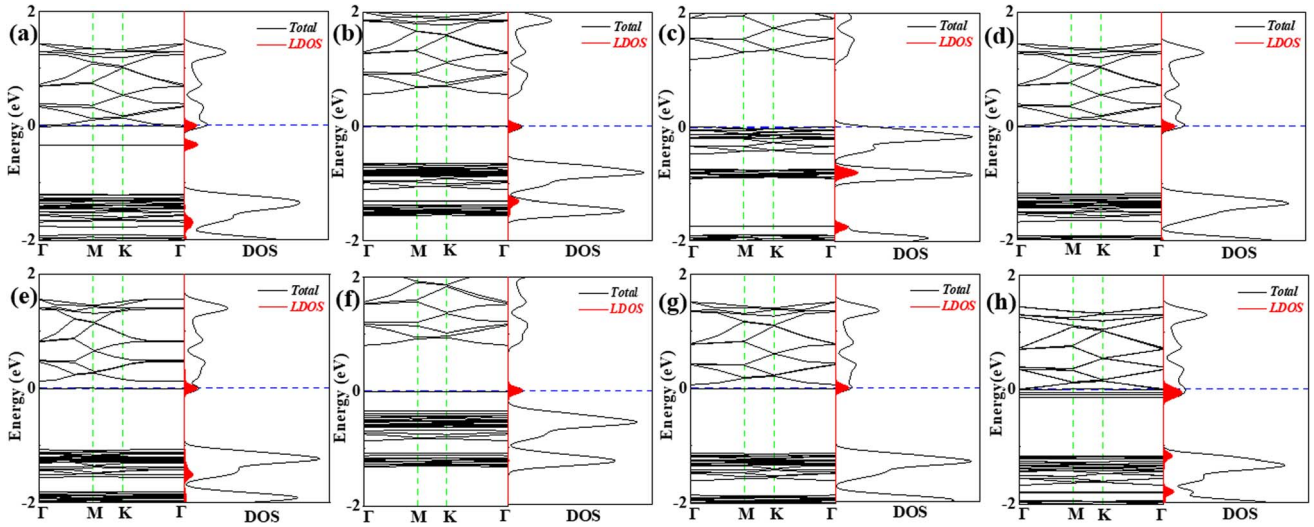

Fig. 6 The BSs and DOSs of the second most stable structure of each VOC molecule on the C_6N_7: (a) toluene-2, (b) benzene-2, (c) vinyl chloride-2, (d) ethane-2, (e) acetone-2, (f) ethanol-2, (g) acetaldehyde-1, and (h) methanal-2. The local DOS (LDOS) of isolated molecules were marked as red under total DOS curves (dark lines).

has comparatively small influence on the BSs and DOSs of the monolayer, however, on the contrary, the adsorption formed by VOC molecules located at in pore center or the edge of the pore remarkably effect on the BSs and DOSs of the C_6N_7 monolayer. Concretely, there are three ways for the adsorption of molecules effect the electronic properties: (1) the adsorption induced by VOC molecules located at the heptazine unit produces some impurity states and occupied states, where the impurity states are mainly located near the Fermi level that results the band gap narrowing mildly while the occupied states locate far away from the Fermi level so that interact with original valence band, leading to strong adsorption (see Fig. 5a–d, and 6c); (2) the

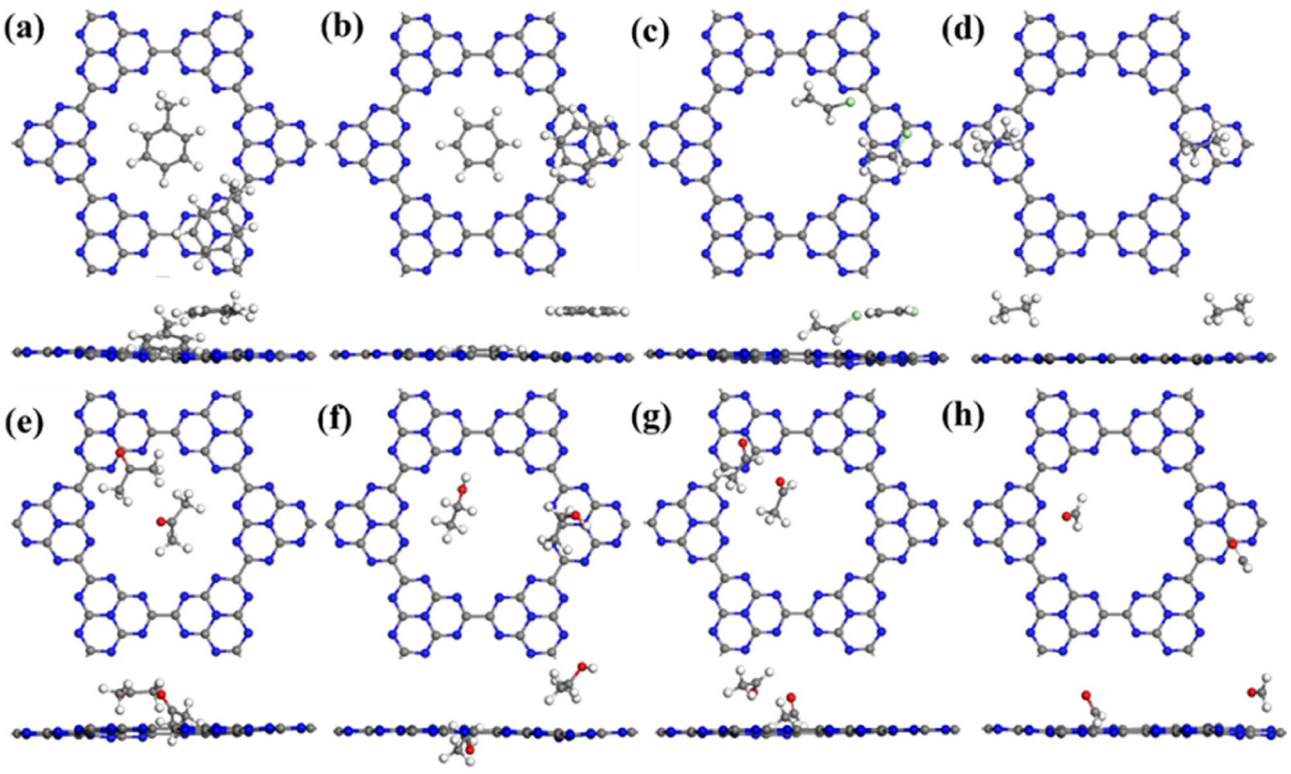

Fig. 7 The most stable structures of VOC molecules co-adsorbed on C_6N_7 monolayer: (a) toluene, (b) benzene, (c) vinyl chloride, (d) ethane, (e) acetone, (f) ethanol, (g) acetaldehyde, and (h) methanal. The local DOS (LDOS) of isolated molecules were marked as red under total DOS curves (dark lines).

Table 2 Average adsorption energy (E_{ad}) and average transferred charge (ΔQ) from molecule to monolayer, band gap (E_g), work function (Φ), sensitivity (S) and recovery time (τ) for VOC molecules co-adsorbed on the C_6N_7 monolayer

System	E_{ad} (eV)	ΔQ (e)	E_g (eV)	Φ (eV)	S	τ (s)
Toluene	−0.886	−0.066	0.005	5.387	8.3×10^9	7.8×10^2
Benzene	−0.743	−0.083	—	5.442	9.2×10^9	3
Vinyl chloride	−0.707	0.014	0.854	6.285	6.1×10^2	0.7
Ethane	−0.422	−0.048	1.189	6.669	5.6×10^{-2}	1.3×10^{-5}
Acetone	−0.704	−0.062	0.005	5.469	8.3×10^9	0.4
Ethanol	−0.614	−0.064	0.116	5.601	9.7×10^8	2.0×10^{-2}
Acetaldehyde	−0.624	−0.034	0.004	5.415	8.5×10^9	3.0×10^{-2}
Methanal	−0.459	0.022	0.092	5.524	1.5×10^9	3.6×10^{-5}

adsorption of VOC molecules that located at the pore edges mainly introduced impurity states, which are located in the original band gap, making the Fermi level shift to these states and narrow the band gap obviously (see Fig. 5e, f, h, and 6f); (3) the adsorption of VOC molecules that locate at in the pore center produced some impurity states that locates near the conduction band, and these adsorption causes the Fermi level moving to the conduction band and making the band gap narrow remarkably, even a transition from semiconducting to conducting properties occurs (see Fig. 6 and Table 1).

Although the VOC molecules can locate at different adsorption sites with slight differences in adsorption energy of 0.015–0.185 eV (see Table 1) expect for ethane, which indicates that the different adsorption locations may co-exist when the concentration of VOC molecules increases, the influence of the adsorption of each VOC molecule at different locations is greatly different from each other. We thus studied the co-adsorption of both of VOC molecules on the C_6N_7 with different adsorption sites, which may illustrate in detail the adsorption behaviors of VOCs as it is on behalf of higher concentration of the VOC gases. The most stable configurations of co-adsorption were shown in Fig. 7, and the corresponding results were summarized in Table 2. Since the adsorption of ethane at the top of pore center is not easy to exist stably (see Fig. 3d), we just considered the most stable sites for ethane. We found that the VOC molecules can stably locate at different locations that are mainly the most and second stable adsorption sites shown in Fig. 2 and 3, respectively. The adsorption energy for VOC molecules is moderate as it falls in the middle of adsorption energies for the most and second stable structures of one VOC molecule on the C_6N_7. More importantly, the influences on the electronic properties of the monolayer induced by different adsorption locations were involved, which were shown in Fig. 8. It is clear that the co-adsorption of VOC molecules (except for vinyl chloride and ethane) has significantly effect on the BSs and DOSs, that is, the induced impurity states by VOC molecules cause the Fermi level shifting to conduction bands and narrowing dramatically the band gap, which is a desirable feature for gas sensing applications. However, the co-adsorption of vinyl chloride and ethane, particularly for ethane changes inconspicuously the electronic properties.

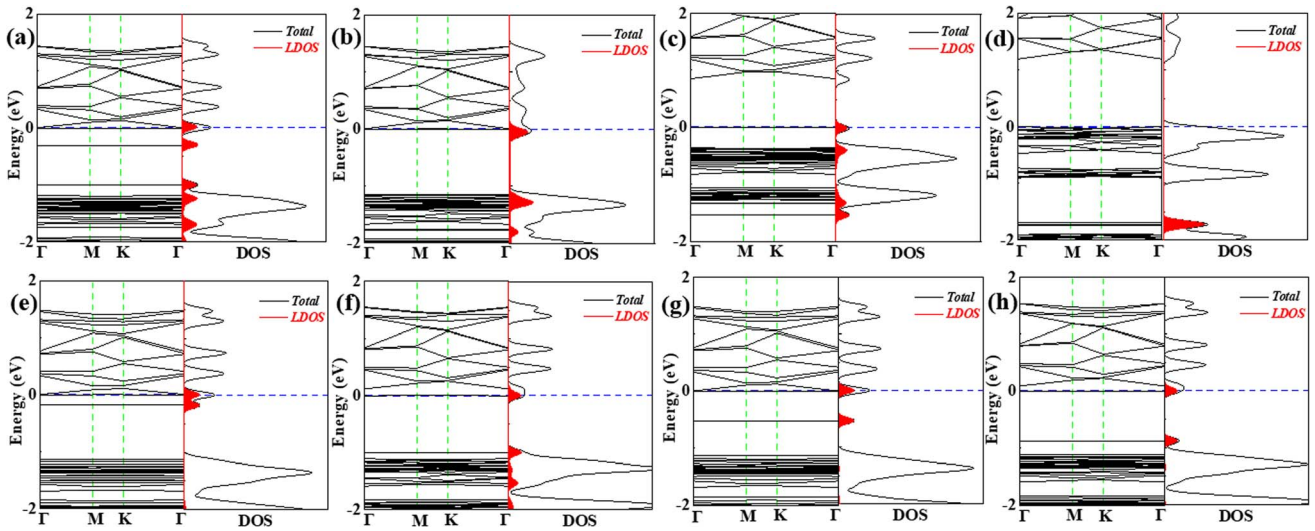

Fig. 8 The BSs and DOSs of VOC molecules co-adsorbed on the C_6N_7 monolayer: (a) toluene, (b) benzene, (c) vinyl chloride, (d) ethane, (e) acetone, (f) ethanol, (g) acetaldehyde and (h) methanal. The local DOS (LDOS) of isolated molecules were marked as red under total DOS curves (dark lines).

Then, we explored the gas-sensing performance of the C_6N_7 monolayer towards the considered VOC molecules. The sensitivity (S) of a resistance-type VOC gas sensor was evaluated bas $S = \left|\frac{G - G_0}{G_0}\right|$,[52,69] where G and G_0 is the electrical conductance of the C_6N_7 with and without VOC adsorption, which is generally stated as $G = AT^{3/2}e^{\frac{-E_g}{2kT}}$,[48] where A a constant, T the temperature, and k the Boltzmann constant. Based on these equations, the calculated sensitivities for VOC molecules were shown in Table 2. As mentioned above, the adsorption of toluene, benzene, acetone, ethanol, acetaldehyde, and methanal causes the band gap of the monolayer decreasing form 1.187 eV in original state to the range of 0.005–0.116 eV (see Table 2), indicating that the C_6N_7 monolayer has high sensitivity to these VOCs as a matter of fact that the calculated sensitivities of these VOCs are quite large compared with that of vinyl chloride and ethane.

Further, the sensitivity can be evaluated *via* the change of work function (Φ), which works on a Kelvin oscillator tool.[70] The variation of work functions for VOC molecule adsorption compared to that of the pure C_6N_7 was displayed in Fig. 9. We found that the adsorption of VOCs (toluene, benzene, acetone, ethanol, acetaldehyde, and methanol) leads the Φ of the pure C_6N_7 (6.64 eV) changing into 5.387, 5.442, 5.469, 5.601, 5.415, and 5.524 eV, respectively, corresponding to the variation of 18.9%, 18.0%, 17.7%, 15.6%, 18.5%, and 16.8%, indicating that the C_6N_7 monolayer as these VOC Φ-type sensors has high sensitivity. In addition, the field emission current density (J) can be described by Fowler–Nordheim equation as $J = A(\beta E)^2 \exp(-4\sqrt{2m}\Phi^{3/2}/\beta E)$,[38] where A a constant, β the field enhancement factor, E electric field intensity, and m electron mass. It is clear that the Φ value of the C_6N_7 can be can effectively tuned by the adsorption of VOC molecules, and then the different Φ will produce different field emission abilities *via* the VOCs adsorption. Therefore, the J for the C_6N_7 monolayer induced by the adsorption of different VOC molecules at a certain voltage could be employed to measure the sensitivity and separate these molecules in experiments. These results reveal that the C_6N_7 monolayer as resistance-type and Φ-type gas sensors for VOCs detections is highly sensitive and selective.

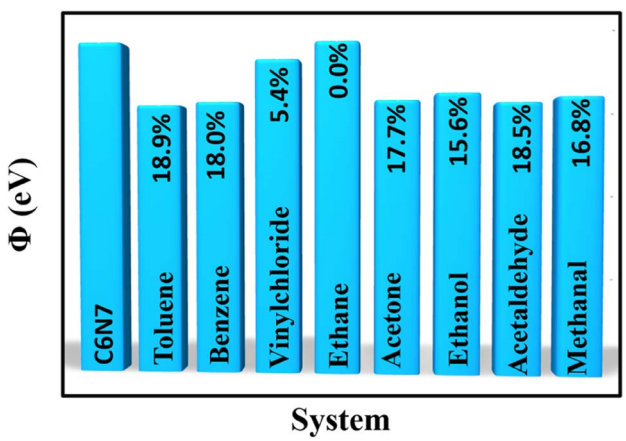

Fig. 9 The work functions for the adsorption of VOC molecules with respect to that of the pure C_6N_7 monolayer.

The recovery time (τ), which means the difficulty of desorption of VOC molecules from the monolayer, was calculated using $\tau = \nu_0^{-1}e^{-E_{ad}/kT}$,[71] where ν_0 is the attempted frequency of VOC molecule in the visible light region (10^{12} s^{-1}). Too-long τ indicates the non-reusability of the C_6N_7-based sensor, but too-short τ causes the sensor no time for responding to the corresponding VOCs. It is found that the τ for benzene, acetone, ethanol, acetaldehyde, and methanal is about 3, 0.4, 2.0×10^{-2}, 3.0×10^{-2}, and 3.6×10^{-5} s at room temperature, respectively, which is appropriate for the desorption of these VOC molecules from the C_6N_7-based sensor, indicating that the C_6N_7-based sensor for the detection of these VOCs is highly reusable at room temperature. At 300 K, the recovery time of toluene was about 7.8×10^2 s, which makes it difficult for toluene to desorb from the C_6N_7 monolayer, and thereby make the C_6N_7-based sensor be inapplicable as reusable gas sensor at room temperature, but a disposable toluene sensor. However, the possibility of using C_6N_7 monolayer as a scavenger for toluene capture and storage is desirable as the strong adsorption strength and long recovery time. In addition, although the recovery time of vinyl chloride and ethane is also desirable (0.7 and 1.3×10^{-5} s, respectively), the sensitivity of the C_6N_7-based sensor towards vinyl chloride and ethane is too low, resulting in incapable of detection of vinyl chloride and ethane at room temperature. Therefore, our research indicates that the C_6N_7 monolayer is capable of high-efficient gas sensors and scavengers for VOCs such as benzene, acetone, ethanol, acetaldehyde, and methanal at room temperature.

It is well known that the commercially available sensors are mainly the amperometric and conductometric types, whose sensing mechanisms are commonly electrochemical or chemiresistive. Tan *et al.*[8] have summarized the sizes of sensing materials, target VOCs, models of original equipment manufacturers (OEM), sensitivity, range of detection, and response time of some major commercially amperometric and conductometric VOCs sensors in the literature review. Compared with these major commercially VOCs sensors, the C_6N_7-based sensor has higher sensitivity and rapid recovery time for the detections of VOCs (benzene, acetone, ethanol, acetaldehyde, and methanal) at room temperature, which remarkably motivates further research on the fabrications of the C_6N_7-based VOC sensors.

4. Conclusions

The detection and removal of volatile organic compounds (VOCs), which are released by different sources, are essential due to their direct impact on human health, environment, and ecosystem. However, the existing VOC sensors remain with many drawbacks like lower sensitivity and selectivity, and unstable room temperature detection. It is thus an imperative need to develop more suitable sensing materials. From this, the adsorption behaviors and gas-sensing characteristics of selective VOC gas molecules (toluene, benzene, vinyl chloride, ethane, methanal, acetone, ethanol, and acetaldehyde) on C_6N_7 monolayers were systematically studied using first-principles methods to explore the possibilities of C_6N_7 monolayers as VOC sensors and scavengers. We found that the physical

adsorption of VOCs (toluene, benzene, acetone, ethanol, and acetaldehyde, and methanol), which was confirmed by ELF plots, is strong enough for the C_6N_7 monolayer as scavengers to removal of these VOCs (The absolute E_{ad} ranging from 0.586 to 0.956 eV). Further, these adsorptions can significantly tune the electronic properties and work function of the C_6N_7 monolayer, indicating that the C_6N_7 monolayer is highly sensitive and selective to these VOC gases. Although the vinyl chloride is also strongly adsorbed on the monolayer, the adsorption barely influence the electronic and optical properties of C_6N_7, showing bad sensitivity of the monolayer to vinyl chloride. Further, the recovery time of benzene, acetone, ethanol, acetaldehyde, and methanal is about 3, 0.4, 2.0×10^{-2}, 3.0×10^{-2}, and 3.6×10^{-5} s at 300 K, indicating that the C_6N_7-based sensor for the detection of these VOCs has high reusability. The recovery time of toluene was about 7.8×10^{2} s at 300 K, which is so long that makes the C_6N_7-based sensor as a disposable toluene sensor. However, the possibility of using C_6N_7 monolayer as a scavenger for toluene capture and storage is desirable as the strong adsorption strength and long recovery time. Therefore, our work confirm that the C_6N_7 monolayer as reusable resistance-type and Φ-type gas sensors and scavengers are high sensitive and selective to VOCs such as benzene, acetone, ethanol, acetaldehyde, and methanal, but a disposable toluene gas sensors and scavenger at room temperature.

Conflicts of interest

There are no conflicts of interest to declare.

Acknowledgements

This work is supported by the National Natural Science Foundation of China (No. 61774056), the Young Backbone Teacher in Colleges and Universities of Henan Province (No. 2020GGJS076), and Longmen Laboratory (No. LMZDKT2022001).

References

1 V. Galstyan, A. D'Arco, M. D. Fabrizio, N. Poli, S. Lupi and E. Comini, *Rev. Anal. Chem.*, 2021, **40**, 33–57.
2 R. J. Rath, S. Farajikhah, F. Oveissi, F. Dehghani and S. Naficy, *Adv. Eng. Mater.*, 2023, **25**, 2200830.
3 H. Li, S. Zhao, S. Zang and J. Li, *Chem. Soc. Rev.*, 2020, **49**, 6364–6401.
4 K. R. B. Singh and R. P. Singh, *Nanosensors for Environment, Food and Agriculture*, 2021, **1**, 229.
5 M. Khatib and H. Haick, *ACS Nano*, 2022, **16**, 7080–7115.
6 R. A. B. John and A. R. Kumar, *Inorg. Chem. Commun.*, 2021, **133**, 108893.
7 R. Epping and M. Koch, *Molecules*, 2023, **28**, 1598.
8 W. C. Tan and K. W. Ang, *Adv. Electron. Mater.*, 2021, **7**, 2001071.
9 L. Wang, Y. Cheng, S. Gopalan, F. Luo, K. Amreen, R. K. Singh, S. Goel, Z. Lin and R. Naidu, *ACS Sens.*, 2023, **8**, 1373–1390.
10 Y. R. Kumar, K. Deshmukh, T. Kovářík and S. K. K. Pasha, *Coord. Chem. Rev.*, 2022, **461**, 214502.
11 A. Behera, S. R. Mahapatra, S. Majhi, N. Misra, R. Sharma, J. Singh, R. P. Singh, S. S. Pandey, K. R. B. Singh and R. G. Kerry, *Environ. Res.*, 2023, **234**, 116556.
12 J. Patel, K. R. B. Singh, A. K. Singh, J. Singh and A. K. Singh, *Environ. Res.*, 2023, **235**, 116674.
13 S. Yang, C. Jiang and S. Wei, *Appl. Phys. Rev.*, 2017, **4**, 021304.
14 Z. Meng, R. M. Stolz, L. Mendecki and K. A. Mirica, *Chem. Rev.*, 2019, **119**, 478–598.
15 J. Cao, Q. Chen, X. Wang, Q. Zhang, H. Yu, X. Huang and W. Huang, *Research*, 2021, **2021**, 9863038.
16 D. J. Buckley, N. C. G. Black, E. G. Castanon, C. Melios, M. Hardman and O. Kazakova, *2D Mater.*, 2020, **7**, 032002.
17 Y. Liu, X. Dong and P. Chen, *Chem. Soc. Rev.*, 2012, **41**, 2283–2307.
18 C. I. L. Justino, A. R. Gomes, A. C. Freitas, A. C. Duarte and T. A. P. Rocha-Santos, *TrAC, Trends Anal. Chem.*, 2017, **91**, 53–66.
19 Z. D. Leve, E. I. Iwuoha and N. Ross, *Materials*, 2022, **15**, 1326.
20 Q. Feng, B. Huang and X. Li, *Adv. Funct. Mater.*, 2021, **31**, 2104058.
21 R. Ghosh, M. Aslam and H. Kalita, *Mater. Today Commun.*, 2022, **30**, 103182.
22 Z. Chen, J. Wang and Y. Wang, *Talanta*, 2021, **235**, 122745.
23 G. K. Walia, D. K. K. Randhawa and K. S. Malhi, *J. Mol. Model.*, 2021, **27**, 277.
24 S. S. Varghese, S. H. Varghese, S. Swaminathan, K. K. Singh and V. Mittal, *Electronics*, 2015, **4**, 651–687.
25 X. Liu, T. Ma, N. Pinna and J. Zhang, *Adv. Funct. Mater.*, 2017, **27**, 1702168.
26 J. Zhang, Y. Chen and X. Wang, *Energy Environ. Sci.*, 2015, **8**, 3092–3108.
27 S. Bu, N. Yao, M. A. Hunter, D. J. Searles and Q. Yuan, *npj Comput. Mater.*, 2020, **6**, 128.
28 J. Mahmood, E. K. Lee, M. Jung, D. Shin, I. Jeon, S. Jung, H. Choi, J. Seo, S. Bae, S. Sohn, N. Park, J. H. Oh, H. Shin and J. Baek, *Nat. Commun.*, 2015, **6**, 6486.
29 L. Tan, C. Nie, Z. Ao, H. Sun, T. An and S. Wang, *J. Mater. Chem. A*, 2021, **9**, 17–33.
30 Z. Tian, N. López-Salas, C. Liu, T. Liu and M. Antonietti, *Adv. Sci.*, 2020, **7**, 2001767.
31 J. Barrio, M. Volokh and M. Shalom, *J. Mater. Chem. A*, 2020, **8**, 11075–11116.
32 S. Kumar, V. R. Battula and K. Kailasam, *Carbon*, 2021, **183**, 332–354.
33 H. Yang, Z. Wang, S. Liu, Y. Shen and Y. Zhang, *Chin. Chem. Lett.*, 2020, **31**, 3047–3054.
34 Y. Yong, H. Cui, Q. Zhou, X. Su, Y. Kuang and X. Li, *Appl. Surf. Sci.*, 2019, **487**, 488–495.
35 A. Wasfi, S. Awwad, M. Hussein and F. Awwad, *Nanomaterials*, 2023, **13**, 700.
36 P. Panigrahi, M. Sajjad, D. Singh, T. Hussain, J. A. Larsson, R. Ahuja and N. Singh, *Appl. Surf. Sci.*, 2022, **573**, 151579.
37 Y. Liu, C. Ye, H. Zhao, K. Lin, X. Cao and Y. Ai, *Crystals*, 2023, **13**, 816.

38 Z. Zhao, Y. Yong, S. Hu, C. Li and Y. Kuang, *AIP Adv.*, 2019, **9**, 125308.
39 S. Agrawal, G. Kaushal and A. Srivastava, *Chem. Phys. Lett.*, 2021, **762**, 138121.
40 K. Ma, Y. Wang, Y. Zheng, J. Xiao, L. Xu, X. Dai and Z. Wang, *Adv. Theory Simul.*, 2023, **6**, 2200611.
41 H. Cui, C. Yan, P. Jia and W. Cao, *Appl. Surf. Sci.*, 2020, **512**, 145759.
42 Y. Yong, W. Zhang, Q. Hou, R. Gao, X. Yuan, S. Hu and Y. Kuang, *Appl. Surf. Sci.*, 2022, **606**, 154806.
43 Y. Yong, S. Hu, X. Yuan, R. Gao, Q. Hou and Y. Kuang, *Int. J. Hydrogen Energy*, 2022, **47**, 29371–29381.
44 H. H. Hammud, M. Yar, I. Bayach and K. Ayub, *Nanomaterials*, 2023, **13**, 1121.
45 W. Zhang, Y. Yong, Z. Li, Z. Li, J. Tao and Y. Kuang, *Surf. Interfaces*, 2022, **33**, 102254.
46 Y. Yong, R. Gao, X. Yuan, Z. Zhao, S. Hu and Y. Kuang, *Appl. Surf. Sci.*, 2022, **591**, 153129.
47 S. Hu, Y. Yong, Z. Zhao, R. Gao, Q. Zhou and Y. Kuang, *Int. J. Hydrogen Energy*, 2021, **46**, 21994–22003.
48 Z. Wang, R. Zhang, Z. Liu, X. Wei, M. Zhao, X. Zhang, Y. Yong, H. Cui and X. Li, *Surf. Interfaces*, 2023, **39**, 102971.
49 X. Yuan, Y. Yong, Q. Hou, S. Hu, R. Gao and Y. Kuang, *Appl. Surf. Sci.*, 2023, **626**, 157090.
50 N. Kumar, M. Kumari, M. Ismael, M. Tahir, R. K. Sharma, K. Kumari, J. R. Koduru and P. Singh, *Environ. Res.*, 2023, **231**, 116149.
51 Y. Yong, F. Ren, Z. Zhao, R. Gao, S. Hu, Q. Zhou and Y. Kuang, *Appl. Surf. Sci.*, 2021, **551**, 149383.
52 S. M. Aghaei, A. Aasi, S. Farhangdoust and B. Panchapakesan, *Appl. Surf. Sci.*, 2021, **536**, 147756.
53 Y. Wang, C. Wu, Y. Tian, L. Yan, H. Tan and Z. Su, *Appl. Surf. Sci.*, 2018, **453**, 442–448.
54 X. Zhao, Y. Zhao, H. Tan, H. Sun, X. Qin, W. Ho, M. Zhou, J. Lin and Y. Li, *Sci. Bull.*, 2021, **66**, 1764–1772.
55 A. Bafekry, M. Faraji, M. M. Fadlallah, I. A. Sarsari, H. R. Jappor, S. Fazeli and M. Ghergherehchi, *Appl. Phys. Lett.*, 2021, **119**, 142102.
56 A. Bafekry, M. Faraji, N. N. Hieu, Y. S. Ang, S. Karbasizadeh, I. A. Sarsari and M. Ghergherehchi, *Nanotechnology*, 2022, **33**, 075707.
57 A. Bafekry, M. Faraji, N. N. Hieu, A. B. Khatibani, M. M. Fadlallah, D. Gogova and M. Ghergherehchi, *Appl. Surf. Sci.*, 2022, **583**, 152270.
58 B. Mortazavi, F. Shojaei, A. V. Shapeev and X. Zhuang, *Carbon*, 2022, **194**, 230–239.
59 B. Mortazavi, F. Shojaei and M. Shahrokhi, *Appl. Phys. Lett.*, 2022, **121**, 056101.
60 B. Delley, *J. Chem. Phys.*, 1990, **92**, 508–517.
61 B. Delley, *J. Chem. Phys.*, 2000, **113**, 7756–7764.
62 J. P. Perdew, A. Ruzsinszky, G. Csonka, O. Vydrov, G. Scuseria, L. Constantin, X. L. Zhou and K. Burke, *Phys. Rev. Lett.*, 2008, **100**, 136406.
63 S. Grimme, *J. Comput. Chem.*, 2006, **27**, 1787–1799.
64 D. R. Hamann, M. Schluter and C. Chiang, *Phys. Rev. Lett.*, 1979, **43**, 1494–1497.
65 H. J. Monkhorst and J. D. Pack, *Phys. Rev. B: Solid State*, 1977, **16**, 1748–1749.
66 F. L. Hirshfeld, *Theor. Chim. Acta*, 1977, **44**, 129–138.
67 S. J. Clark, M. D. Segall, C. J. Pickard, P. J. Hasnip, M. I. J. Probert, K. Refson and M. C. Payne, *Z. Kristallogr.*, 2005, **220**, 567–570.
68 T. Hussain, M. Sajjad, D. Singh, H. Bae, H. Lee, J. A. Larsson, R. Ahuja and A. Karton, *Carbon*, 2020, **163**, 213–223.
69 A. Aasi, S. M. Aghaei and B. Panchapakesan, *J. Mater. Chem. C*, 2021, **9**, 9242–9250.
70 Y. Yong, R. Gao, X. Wang, X. Yuan, S. Hu, Z. Zhao, X. Li and Y. Kuang, *Results Phys.*, 2022, **33**, 105208.
71 S. Peng, K. Cho, P. Qi and H. Dai, *Chem. Phys. Lett.*, 2004, **387**, 271–276.